




Effect of iron content and warm compaction temperature on microstructure evolution and characteristics of the Cu-Ni-xFe based alloys

Suprianto^{1*}, Fajar Pratama Maulana¹, Sigit Budi Prasetyo¹,
M. Sabri¹, Suherman², Reisya Ichwani¹

¹ Department of Mechanical Engineering, Faculty of Engineering, Universitas Sumatera Utara, Jl. Almamater Kampus USU, Padang Bulan, Medan, 20155, Indonesia

² Department of Mechanical Engineering, Faculty of Engineering, Universitas Muhammadiyah Sumatera Utara, Jl. Kapt. Mukhtar Basri No. 3, Medan, 20238, Indonesia

* Corresponding author's e-mail: suprianto@usu.ac.id

ABSTRACT

An electrode is one of the components in the electric discharge machine (EDM), that requires excellent electrical conductivity and strength. This component is typically made of Cu-based alloys which can be synthesized by powder metallurgy (PM). Their strength can be enhanced by the addition of alloy elements and the improvement of specific parameters. In this study, the characteristics of Cu-Ni-xFe alloys including the microstructure evolution, compressive strength, hardness, and electrical properties were investigated with different Fe contents and the compaction temperature. The results show that the addition of Fe tended to increase the hardness and compressive yield strength of the model alloys linearly. The maximum compressive yield strength of 227.16 MPa was obtained for Cu-Ni-3.0 wt.%Fe alloy with 150 °C compaction temperature. The electrical conductivity of all model alloys exceeded 75% IACS, in which alloys with compaction temperatures ranging from 150 to 250 °C showed a higher conductivity. The microstructure of Cu-Ni-xFe alloys was observed to have Cu-Ni solid solution and intermetallic phases, which increased the hardness of the alloys. In conclusion, the addition of Fe element and compaction temperature affect the microstructure, mechanical, and electrical properties of Cu-Ni-xFe alloys.

Keywords: alloys, powder metallurgy, mechanical properties, electrical conductivity.

INTRODUCTION

Cu-based alloys are conductivity alloys that are commonly used in electrical and electronic components, such as electrodes for an electric discharge machine (EDM). The strength may have deteriorated as a result of its frequent use in high-temperature applications. Thus, it is important to improve the strength of alloys.

The mechanical strength of the alloys is affected differently by additional constituents such as Ni, W, Fe, Al, and carbide/oxide particles. The addition of Ni (3 wt.%) has been reported to improve the hardness, compressive strength, and fatigue strength of Al-Cu alloy [1]. The presence of

those additional elements could enhance the hardness of the alloy, which is significant for lowering the alloy's wear rates. Similar to nickel, the addition of W into Cu-Fe alloy has also increased the hardness and wear resistance [2]. Al_2O_3 particles have also been reported to improve the compressive yield strength of the Cu/Cu-Ni alloys [3]. Furthermore, the increase of Fe significantly enhanced the tensile strength of the Cu-Fe alloys synthesized through the powder technique [4].

In terms of strengthening, there are several routes to strengthen Cu-based alloys, such as solid solution, precipitation, and dispersion strengthening. Some strengthening in Cu-based alloys have been reported, including solid solution

strengthening in the Ni-Cu alloys [5], precipitates strengthening in Cu-Ni-Al alloys [6], and oxides particles (Al_2O_3 , Y_2O_3 , and ZrO_2) strengthening in the Cu-based alloys [7].

The addition of alloy elements into Cu-Ni alloy has contributed to improve their strength. However, increasing the alloy elements tends to reduce their electrical conductivity. It has been reported that the addition of W up to 30 wt.% reduced the %IACS to below 60% [8]. In the W-Cu alloy system, Cu has an important role in increasing the electrical conductivity of the alloy, while it reduces their resistivity [9]. The presence of Al in the Cu-Ni-Si causes a slight decrease in the electrical conductivity [3]. Similar to this element, the increase of Ni in the Cu-0.4Be alloy has been reported to decrease its conductivity; however, the conductivity was improved by the aging process at 400 °C [10]. Furthermore, the presence of both Ni and Mn in the Cu-Ni-Mn-P alloys produced by melt-hot rolling-aging has been observed to reduce the alloys' conductivity [11].

Powder metallurgy can be used to fabricate various materials, such as Fe-Cu [12], Fe-Cu-Ni-Sn composite reinforced by CrB_2 and VN particles [13], and Cu-Ni alloys [14]. The process parameters in powder metallurgy like compaction pressure and sintering temperature are important. Those parameters have been observed to influence the densification and distortion of the Cu-Sn-Pb alloys during sintering [15]. The pressure (200~1200 MPa) has enhanced the density, yield strength, and hardness of the TiH2-185 alloys [16]. Enhancing the compressive strength of both the Al-Cu alloys was obtained by increasing the compaction pressure [17]. Those compressive loads along with the sintering temperature have also influenced the electrical conductivity of the Cu-Ni-W alloys [18].

In powder metallurgy, warm compaction has been applied in varying model alloys such as Fe-Cu-Ni-Mo-C [19], Cu-based [20], C-Cu composites for electrical components [21], and magnetic powder cores material [22]. A compaction temperature between 90 to 150 °C has been applied in the Fe-based alloy. The result shows that the compaction temperature has influenced the density of the alloy [23]. The higher density and wear resistance in Fe-Al alloys were obtained with higher compaction temperatures up to 500 °C [24]. Even though the compaction process has brought positive effects in alloys, careful consideration of the most suited compaction temperature is important

to avoid oxidation of consisted elements in the alloys. The incorporation of temperature during the compaction process of powder metallurgy has been reported in several studies. However, the application of warm compaction in powder metallurgy technique in the Cu-Ni-xFe alloy fabrication used for EDM electrodes is limited. The major problem during the fabrication of Cu-Ni-xFe alloy through powder metallurgy is selecting the right compaction temperature. The excessive compaction temperature potentially increases the oxide formation in the alloy, which interferes with the sintering process and reduces the mechanical as well as the electrical properties of Cu-Ni-xFe alloy. Therefore, this study analyzes the role of the additional Fe contents in Cu-Ni-xFe alloy and the role of varying compaction temperature in Cu-Ni-xFe alloy fabrication through powder metallurgy technique. The microstructure evolution, compressive strength, hardness, and electrical properties of the resulting Cu-Ni-xFe alloy were investigated.

MATERIALS AND METHODS

Metal powders (Cu, Ni, and Fe) with purity of higher than 99.00% and particle size of 30~40 μm have been used as the base material to synthesize Cu-Ni-xFe model alloys through powder metallurgy technique. The detailed composition of each of the elements in the model alloys, as well as the temperature of warm compaction during the fabrication process, are shown in Table 1. The samples were named as 1-A, 2-A, 3-A, 4-B, 5-B, 6-B, and 7.

The first stage of alloy fabrication involved mixing Cu and Ni powders at a weight ratio of 90:10. Furthermore, Fe elements were added into the mixed Cu-Ni powders with different amounts of 0.5, 1.5, 2.5, and 3.0 wt.%. This step was carried out in the glove box under an argon atmosphere to prevent any excessive contaminants. All of the powders are milled by horizontal milling with a 10:1 ball-to-powder ratio (BPR) at the speed of 300 rpm for 2 h. After the mixing process, the powders were compacted with a warm compaction process with a 250 MPa load for 15 minutes holding time at varying temperatures of 120, 150, 200, and 250 °C. Furthermore, the resulting bulk material was sintered at 770 °C for 60 minutes holding time. The characteristics of the resulting model alloys were investigated by different routes including the microstructure

Table 1. The composition of the model Cu-Ni-xFe alloys

Samples	Model alloys	Composition (wt.%)		Warm compaction temperature (°C)
		90Cu10Ni	Fe	
1-A	Cu-Ni-0.5Fe-T ₁₂₀	99.5	0.5	120
2-A	Cu-Ni-1.5Fe-T ₁₂₀	98.5	1.5	120
3-A	Cu-Ni-2.5Fe-T ₁₂₀	97.5	2.5	120
4-B	Cu-Ni-3.0Fe-T ₁₅₀	97	3.0	150
5-B	Cu-Ni-3.0Fe-T ₂₀₀	97	3.0	200
6-B	Cu-Ni-3.0Fe-T ₂₅₀	97	3.0	250
7	Cu-Ni-3.0Fe-T _{room}	97	3.0	Room temperature

evolution, compressive strength, hardness, and electrical properties.

Mechanical testing has been done to observe the compression yield strength of the model alloys with 9.53 mm diameter and 25.53 mm length samples. This testing was conducted using a 5 kN/min loading rate. Furthermore, the Vickers hardness tests with 100 g loading for 30 s were conducted at room temperature. A relative density of model alloys was attained by the Archimedes principle. The X-ray diffraction Rigaku type Mini Flex 600 with Cu- K α radiation model HyPix-400 MF 2D hybrid pixel array detector (HPAD) was used to investigate the crystal structure of the model alloys in powder stages and resulting bulk alloys. The microstructure, elemental distribution, and fracture morphologies of the model alloys were also observed by optical microscope (OM) and scanning electron microscope (SEM) with different magnifications. The samples for OM and SEM observation were 25 mm in diameter and 8 mm in thickness. The surfaces of alloys were prepared

using a polishing machine with SiC grinding paper from 100 to 2000 grit without etching.

RESULTS AND DISCUSSION

X-ray diffraction powder stage of model alloy

Figure 1 shows the XRD spectra of four model Cu-Ni-xFe alloys with different Fe contents (0.5~3.5 wt.%). The main peaks of alloys consisted of Cu elements with fcc crystal structures which have (111), (200), and (220) crystal planes dispersed at the 2 θ of $\sim 43^\circ$, $\sim 51^\circ$, and $\sim 74^\circ$, respectively. The Ni elements with lower peaks dispersed near the Cu peaks were observed. These results were in good agreement with the alloy's design, as shown in Table 1. The XRD results confirmed that Ni and Cu elements have similar fcc crystal structures and crystal planes.

Due to their small amount in the model alloy, the spectra of Fe elements were hardly detected

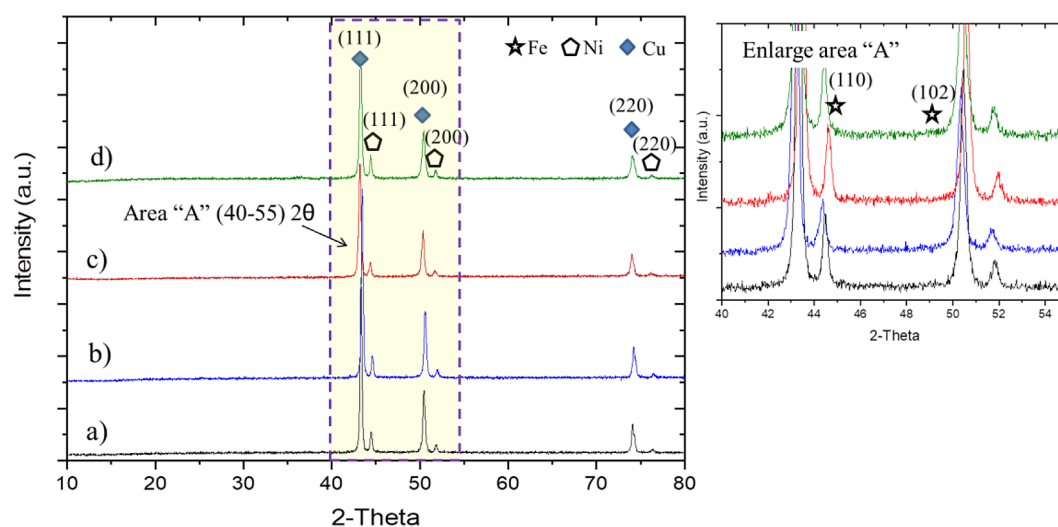


Figure 1. XRD spectra powder stage of the model Cu-Ni based alloys for difference Fe contents; a) 0.5 wt.%, b) 1.5 wt.%, c) 2.5 wt.%, and d) 3.0 wt.%

by XRD, as shown in Figure 1(a-d). However, Figure 1 (enlarged area “A”) at 40–45 of the 2 θ revealed an additional Fe element with (110) and (102) crystal planes. Those planes were dispersed near the root peaks of the Ni and Cu. Furthermore, a slight shift of Ni peaks was observed with the addition of different Fe amounts. The presence of Fe element in the Cu-Fe alloys promoted peak transformation including the 2 θ positions, shapes, and intensities [25]. The Ni peak shifting has been reported with the increasing of the Cu element in the Cu-Ni model alloy [26]. Furthermore, Cu main peaks are still in their position presented in Figure 1. In the powder stages, a significant peak change of the Cu-based alloys has been observed with different milling times in the ball milling method [27]. However, in this current study, there are no different parameters in their mixing process. Thus, the XRD spectra of model alloys are not changed significantly.

The relative density

The various composition and warm compaction temperatures contributed to the relative density (RD) of each sintered model alloy, as depicted in Figure 2. The RD of model alloys was likely to decrease with the increment of the additional Fe contents in the alloy from 82.7% to 79.6% for Cu-Ni-0.5 wt.%Fe-T₁₂₀ (sample 1-A), Cu-Ni-1.5Fe-T₁₂₀ (sample 2-A), and Cu-Ni-2.5Fe-T₁₂₀ (sample 3-A) alloys. Those samples were subjected to 120 °C of warm compaction temperature.

These results correlated with their initial densities of the constituent elements, in which the density of Cu was higher than Fe. In this case, the compaction temperature of 120 °C was observed to not have a significant effect on the density of Cu-Ni-xFe alloys (sample 1-A, 2-A, and 3-A).

Various warm compaction has been applied in the model alloys of Cu-Ni-3.0Fe-T₁₅₀ (sample 4-B), Cu-Ni-3.0Fe-T₂₀₀ (sample 5-B), and Cu-Ni-3.0Fe-T₂₅₀ (sample 6-B). It can be seen in Figure 2 that a slightly different density was observed for different warm compaction in the alloys with temperatures of 150, 200, and 250 °C. Compared to the control alloy of Cu-Ni-3.0Fe-T_{room} (sample 7) with low RD of 78%, the incorporation of the warm compaction to the alloy has successfully increased the RD to 84, 85.4, and 86.3% for 150, 200, and 250 °C temperature, respectively. Trends of increasing relative density by introducing warm compaction have been observed in different materials, such as Cu/CNTs [28] and Al6061/SiC [29]. The higher compaction temperature might generate better particle interlocking and reduce the particle gap of green compaction, which influences the alloy densification process. In the Cu-based alloy system, the relation between warm compaction and density of alloy was also reported in the Fe-Cu-Ni-Mo-C [19]. Similar to the compaction load (250 MPa) applied in this current study, the introduction low compaction load (< 318.47 MPa) has been reported to increase NiTi density significantly. It is correlated with the dislocation phenomenon, subsequent particle interlocking,

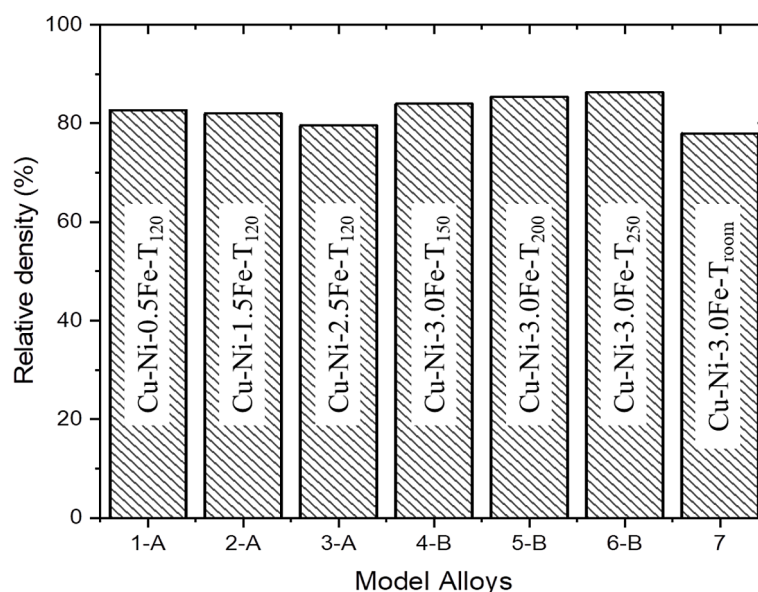


Figure 2. Relative density of the model alloys for different Fe contents and compaction temperature

and void collapse [30]. Although the compaction temperature positively influenced the density of the alloys, higher compaction temperatures posed a risk of oxide formation within the alloy, particularly in reactive elements.

Microstructure of the model alloys

The microstructure of the Cu-Ni-xFe alloy with different Fe contents and compaction temperature were observed by optical microscope, as seen in Figure 3. It is visible that the Cu-Ni-xFe alloy mainly consisted of three different phases, including Cu-rich, Cu-Ni phase, and oxides (referred to bright, light gray-green and dark areas respectively). The presence of Fe element promoted smaller oxide with a particle size of $< 5 \mu\text{m}$ that was dispersed within the Cu-rich/Cu-Ni phases, as seen in Figure 3(c). The favorable affinity of Fe towards oxygen (O) facilitated the formation of Fe-oxides. The porosities were also formed in the sintered model alloys with a few microns in size. In Figure 3 (d-e), small oxides, pores, and solid solution were obtained in Cu-Ni-3.0 wt.%Fe model alloys, but the incorporation of warm temperature during powder compaction into Cu-Ni-3.0 wt.%Fe model alloys did

not significantly change the microstructure. The compaction at room temperature shows the larger particles in the alloy, captured in Figure 3(g).

Figure 4 shows the SEM observation of Cu-Ni-xFe alloy with different Fe contents. From the figures, it is observed that the microstructure mainly consists of solid-solution Cu-Ni and Cu-rich phases, which are indicated by light grey areas.

Figure 4 is the SEM images of the Cu-Ni – xFe model alloys with different Fe element compositions. The increasing of the Fe elements till 3.0 wt.%Fe has been observed to promote more dark grey area in the alloy as shown in Figure 4(a-d), which was likely the formation of Fe-intermetallic phases. The presence of those intermetallic phases enhanced the hardness of the model alloy by restricting the dislocation movement [31]. In this current study, most particle sizes were observed to be less than $5 \mu\text{m}$ with irregular shapes formed as shown in Figure 4(d). Clustered particles and pores were also observed in the SEM images. Though the intermetallic phase increased the brittleness of the alloys, the presence of pores has been reported to decrease the hardness of Cu-Ni-MX1480 [32].

Furthermore, the constituent elements of each phase in the microstructure of the Cu-Ni-xFe alloy

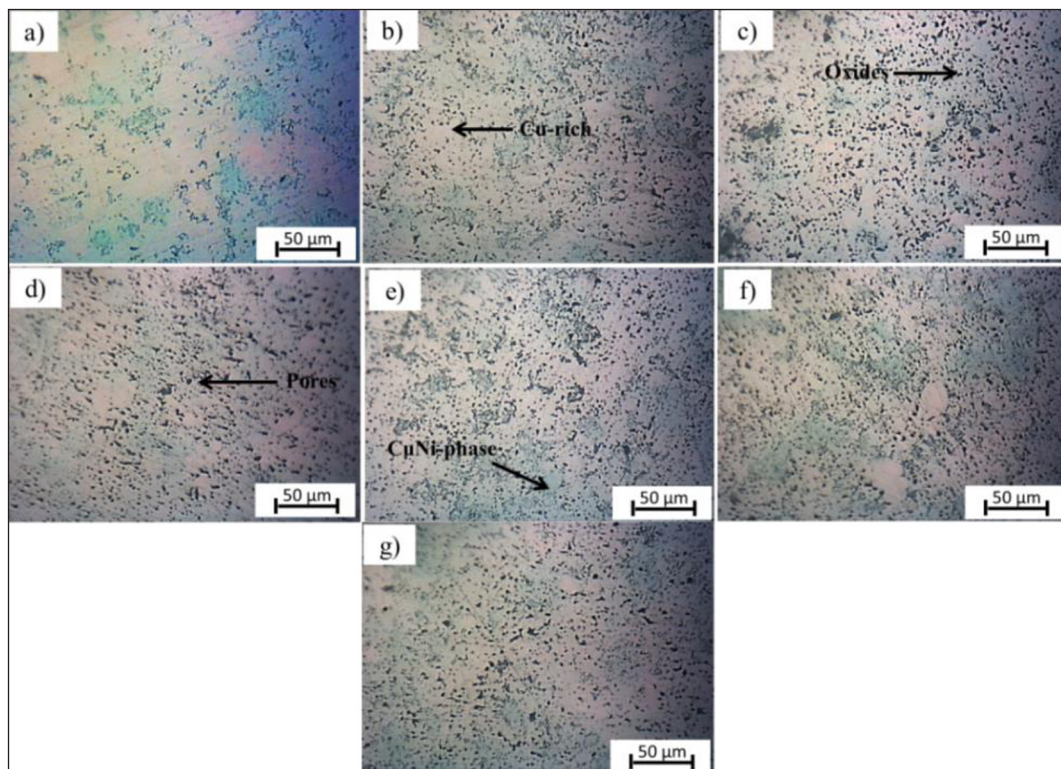


Figure 3. Optical micrographs of the model alloy for different Fe contents (a) 0.5 wt.%Fe, (b) 1.5 wt.%Fe, (c) 2.5 wt.%Fe, and 3.0 wt.%Fe alloy with (d) 150°C, (e) 200°C, (f) 250°C, (g) room temperature compaction

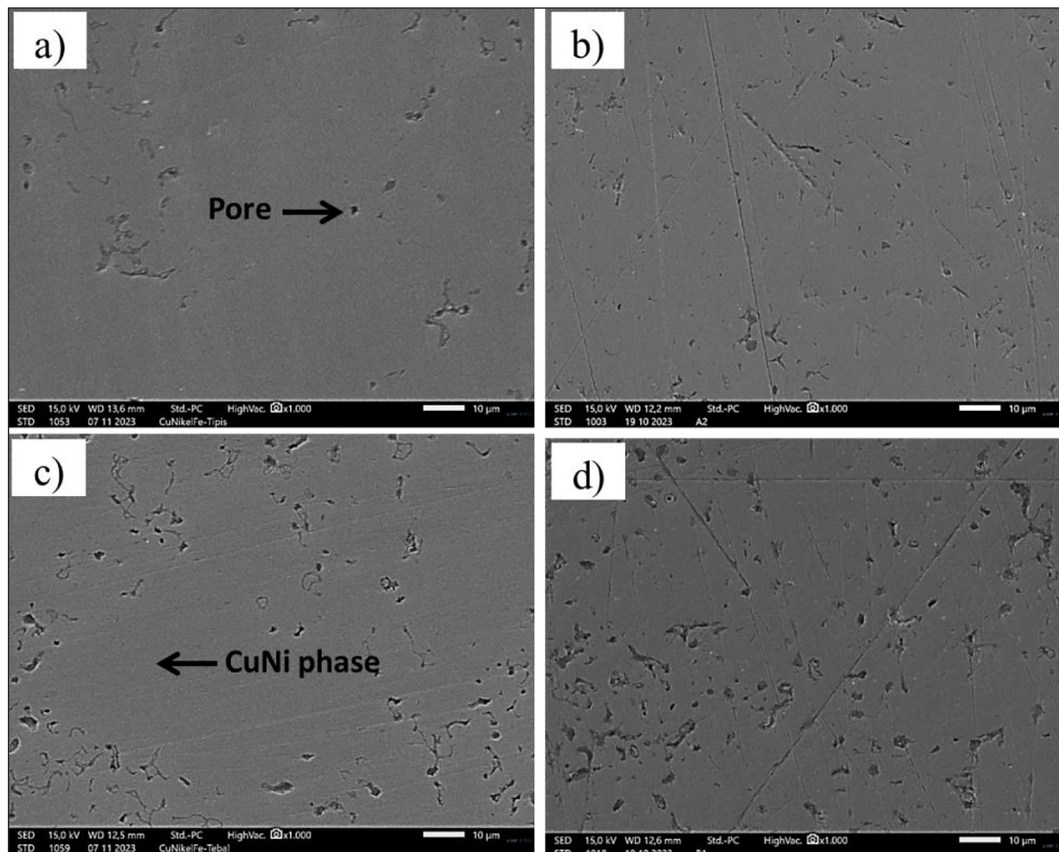


Figure 4. SEM images of the model Cu-Ni-xFe alloys with 120 °C; (a) 0.5Fe, (b) 1.5Fe, (c) 2.5Fe, and (d) 3.0 wt.%Fe with 250 °C warm compaction temperature

were analyzed by energy dispersive spectroscopy (EDS) as illustrated in Figure 5. Figure 5(a) shows the selected surface of Cu-Ni-0.5 wt.%Fe alloy. Area “A” and point “B” in Figure 5(a) were identified as the matrix and pores of the Cu-Ni-0.5 wt.%Fe alloy. The area consisted of Cu element as a main element in the model alloy followed by Ni, Fe, and oxygen elements shown in Figure 5(b-c). In the matrix area (point “A”), the amount of the Cu, Ni, and Fe elements were 90.2 ± 1.10 , 9.29 ± 0.31 , and 0.1 ± 0.03 wt.%, respectively. Detailed information on the element composition of alloy detected by EDS is shown in Table 2. These results correspond well with the alloy composition in Table 1. Furthermore, a weak peak of the oxygen (0.5 ± 0.03 wt.%) was also detected in the matrix area (Fig. 5c). A slight increment up to 3.5 ± 0.09 wt.% of the oxygen was found, as depicted in the enlarged area “A” in Figure 5(b). The oxygen dissolved within the microstructure likely occurred during the powder handling. Detailed composition of all elements in Cu-Ni-xFe model alloys from Figure 5 and Figure 6 are listed in Table 2.

Figure 6 shows the results of SEM and EDS of Cu-Ni alloys with 2.5 wt.%Fe alloy and 1.5 wt.%Fe. In Figure 6(a), The areas of “C” and “D” with small and free pores respectively, containing Cu-rich elements. The presence of this Cu-rich element was also confirmed by EDS, as seen in Figure 6(b). The increase of the Fe element to the alloy till 2.5 wt.%Fe caused a slight increment of the Fe detected in EDS with a peak intensity of > 20.000 . The selected “C” area has a small size porosity of less than $1\mu\text{m}$ dispersed in Cu-Ni matrix, and a small amount of oxygen (0.4 ± 0.03 wt.%). It is indicated by a weak peak captured near the overlapping Cu-Ni-Fe peaks as shown in Figure 6(c).

Furthermore, the EDS observation has been also done in the larger areas (“E”) of the Cu-Ni-1.5 wt.%Fe alloy as seen in Figure 6(d). Elements of Cu, Ni, Fe, O, and C were detected in that area. As listed in Table 2, the amount of the primary Cu, Ni, and Fe elements slightly decreased in the model Cu-Ni-1.5Fe- T_{120} alloy. It is believed that the detected contaminants such as carbon and oxygen about 3.4 ± 0.08 wt.% and 1.2 ± 0.05 wt.% on the alloy influenced the decrease of those total main elements. The presence of carbon probably

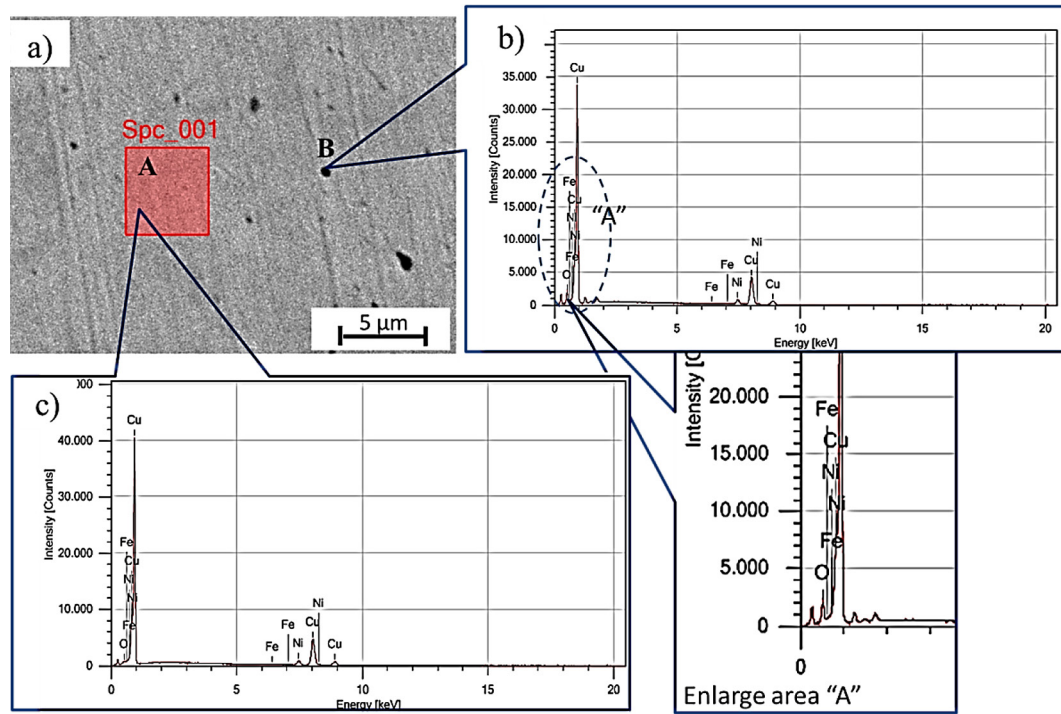


Figure 5. (a) SEM image, (b) and (c) EDS spectra of the model Cu-Ni-0.5 wt.%Fe alloy for different areas

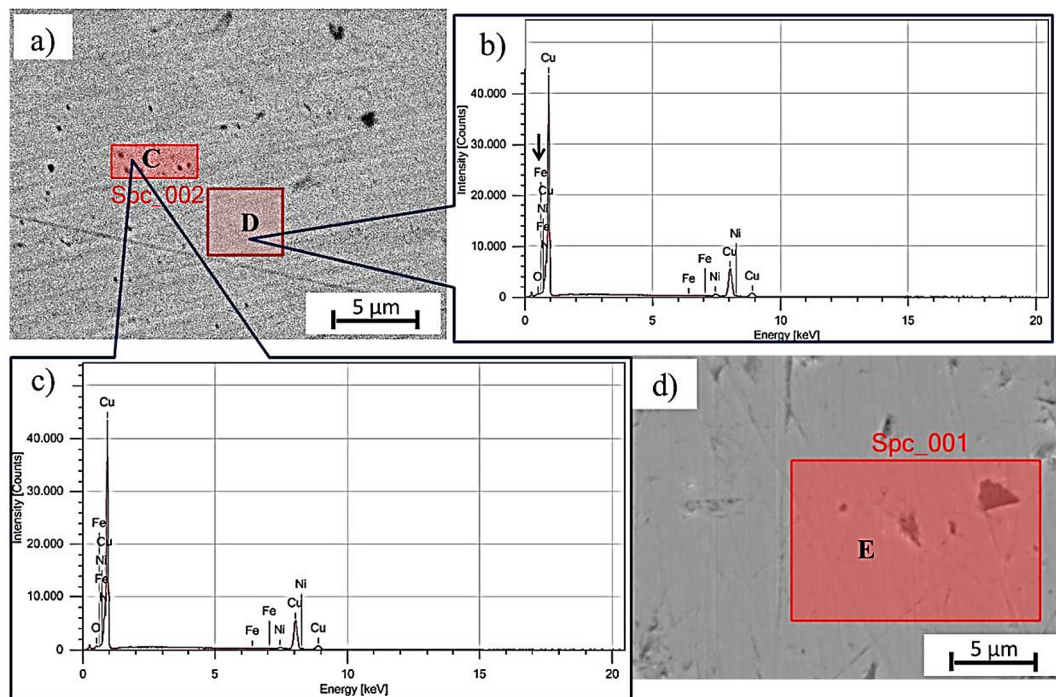


Figure 6. (a) SEM images of the Cu-Ni-2.5 wt.%Fe alloy, (b-c) EDS spectra of the model Cu-Ni-2.5 wt.%Fe alloys, and (d) SEM image and EDS selected area of the Cu-Ni-1.5 wt.%Fe

originated from the grinding media that was made of hard steel and oxygen. Those elements were dissolved into the green material during the powder stages. Moreover, the EDS results also confirmed that contaminants like O and C were preferred to

spread out near pores and oxide areas of the model alloys. The existence of oxygen has been reported to generate pores in the microstructure and reduce the alloy's density [33]. Conversely, carbon contamination is influenced by the sintering

Table 2. The composition of the selected area of the Cu-Ni-xFe model alloys is in Fig. 5 and 6

Model alloys	Are-as	Composition of elements									
		Cu		Ni		Fe		O		C	
		(wt.%)	Error	(wt.%)	Error	(wt.%)	Error	(wt.%)	Error	(wt.%)	Error
Cu-Ni-0.5Fe-T ₁₂₀	A	90.2±1.10	0.16	9.3±0.31	0.16	0.1±0.03	0.11	0.5±0.03	0.11	-	-
	B	86.5±1.12	0.77	10.0±0.33	0.01	0.1±0.03	0.11	3.5±0.09	0.87	-	-
Cu-Ni-2.5Fe-T ₁₂₀	C	95.3±1.07	2.61	4.3±0.20	1.82	-	-	0.4±0.03	0.13	-	-
	D	94.5±1.05	1.70	5.1±0.21	1.16	<0.1±0.02	0.62	0.3±0.03	0.08	-	-
Cu-Ni-1.5Fe-T ₁₂₀	E	88.7±1.06	0.02	5.7±0.23	0.82	1.0±0.07	0.11	1.2±0.05	0.24	3.4±0.08	0.67

temperature, with higher sintering temperatures promoting carbon diffusion and affecting grain growth within the alloy [34].

Elemental mapping on Cu-Ni-0.5 wt.%Fe model alloy with 120 °C compaction temperature has been done as illustrated in Figure 7. The figures clearly show that the Cu-rich elements are homogeneously distributed within the microstructure, as indicated by the bright areas in Figure 7(a-b). Nickel element with 10 wt.% ratio to Cu was dispersed in the same area with Cu, potentially forming a solid solution. Furthermore, a small amount of the Fe element was also detected in the microstructure. Oxygen which acts as contaminants in the model alloy has been recognized over the dark grey and predominantly in the pores, which are in points 1 to 3 in Figure 7(a, e). The EDS mapping has also been done for the Cu-Ni-2.5 wt.%Fe alloys as shown in Figure 8. The elements of Cu and Ni were seen in most areas of the surfaces (Fig. 8(b, c)). The increase of the Fe elements in the model alloy did not significantly influence the distribution of both Cu and Ni elements. However, the segregation of the

Fe and oxides, and some porosities were observed within the microstructure, as seen in the area 1, 2, and 3 in Figure 8. Segregation of the oxide is influenced by the temperature and they are located in the grain boundaries [35]. Other than temperature, this segregation phenomenon might be influenced by many factors such as milling and powder handling. The presence of oxides might be generated at high-temperature conditions, in which high temperature causes the oxygen to be easier to diffuse [36].

X-ray diffraction of the sintered model alloys

X-ray diffraction has also been performed for the sintered model alloys. Figure 9 displays the XRD spectra of sintered model Cu-Ni-based alloys for different Fe contents. The sintered model alloys consisted of main peaks dispersed at 43.94, 50.76, and 74.67° of 2 θ , which were identified as α -(Cu-Ni) rich phases. Near the 2 θ of 43.94°, the overlapping peaks at 43.34° and 43.53° were observed that represented the individual Cu-element and FeNi-intermetallic. The

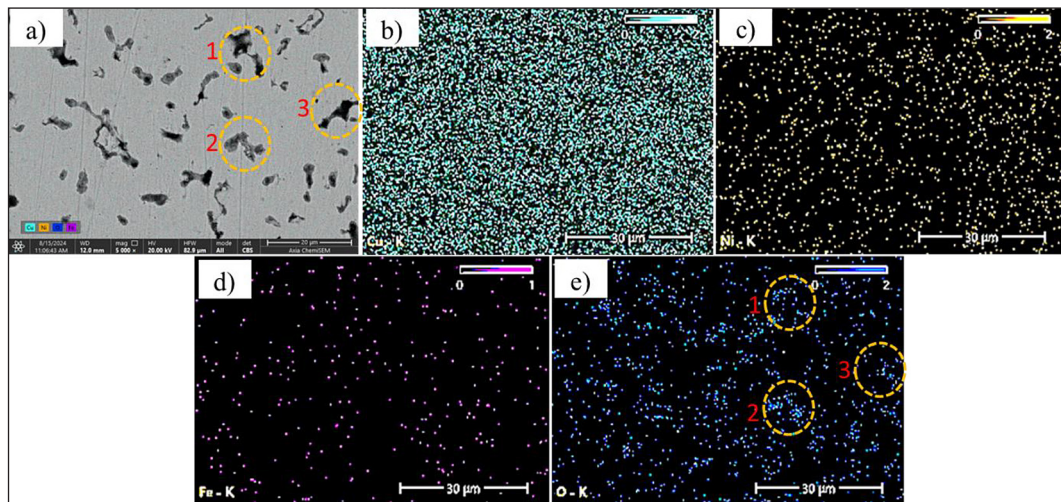


Figure 7. (a) SEM images and (b-e) EDS mapping of the elemental model Cu-Ni-0.5 wt.%Fe alloy synthesized by 120 °C compaction temperature

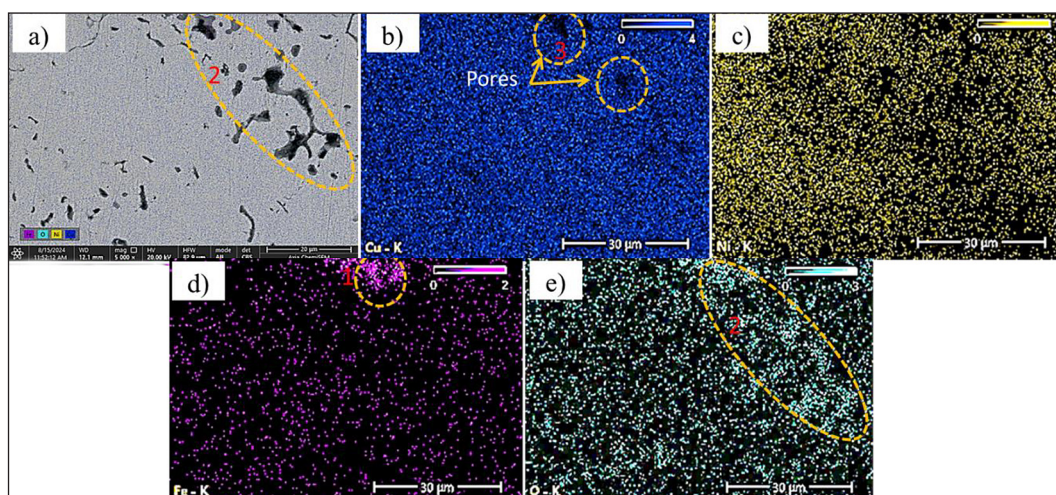


Figure 8. (a) SEM images and (b-e) EDS mapping of the elemental model Cu-Ni-2.5 wt.%Fe alloy synthesized by 120 °C compaction temperature

FeNi intermetallic was formed between CuNi solid solution caused by the small amount of Fe presence. These FeNi intermetallic phases also influenced the mechanical properties of the alloy [37]. It is believed that other intermetallic phases such as Fe_3Ni_2 and FeNi_3 have formed in the model alloys. Even though the Cu-elements were still observed in the sintered alloys, the α -(Cu-Ni) solid solution phases were predominantly in the model alloys. During the high-temperature sintering, Ni atoms are consumed to form α -(Cu-Ni) solid solution phases, which causes the individual Ni peaks to disappear.

Furthermore, the increase of the Fe elements from 0.5 wt.% to 3.0 wt.% subsequently reduced

the intensity peak of Cu elements. It can be seen in Figure 9, that the addition of the iron caused a slight decrease in the intensity of the α -(Cu-Ni) solid solution phase. It might be correlated with the atomic weight of each element in this model alloy, in which the Fe element has a lower atomic weight compared to other elements. The increase of the Fe contents also shifted the peaks to the right side. It is likely correlated to the presence of the O and C contaminants detected in the EDS results (Table 2). Those contaminants in the model alloys caused some Fe-oxides or carbides to be hardly identified by XRD. It is believed that Fe-oxides or carbides peaks might be dispersed in the root peaks.

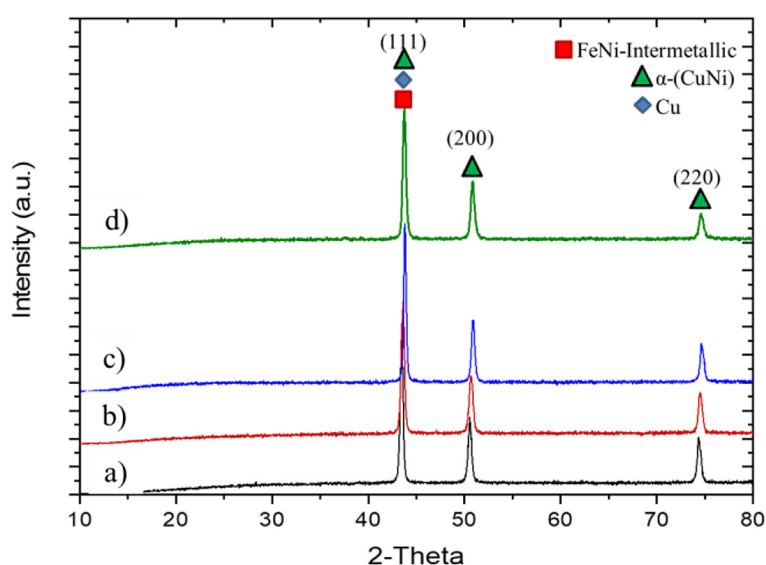


Figure 9. XRD spectra sintered of the model Cu-Ni-based alloys for different Fe contents; (a) 0.5 wt.%, (b) 1.5 wt.%, (c) 2.5 wt.%, and (d) 3.0 wt.%

Mechanical properties of the model alloys

The mechanical properties of the model alloys obtained by Vickers's hardness testing are presented in Figure 10. The addition of Fe into Cu-Ni-based alloy synthesized by 120 °C compaction temperature has promoted a slight increase in alloys' hardness from 50.4, 51.8, and 57.2 HV for 0.5, 1.5, and 2.5 wt.%Fe model alloys (sample 1-A, 2-A, and 3-A, respectively). These results confirmed that the additional Fe contributed to the hardness improvement of the alloys.

Furthermore, the applied warm compaction temperature has improved the densification of the model alloys. The compaction temperature has been reported to cause ductile deformation in Cu powders [38], improve the relative density of the alloy, and reduce pores in the alloy's microstructure [39]. These factors contributed to the high hardness of the alloy. According to the hardness results in Figure 10, it can be concluded that the compaction temperature has significantly affected the hardness of the model Cu-Ni alloys with low Fe contents. The compaction temperature has increased the alloys' hardness. The Cu-Ni-3.0 wt.%Fe alloy with compaction temperature at 250 °C has the highest hardness of 63.7 HV, while the Cu-Ni-3.0 wt.% Fe alloy with compaction at room temperature has the lowest hardness of 52.7 HV.

The compressive yield strength of the model alloys has also been investigated. Figure 11

shows the obtained compressive yield strength of the model alloys with different Fe contents and warm compaction temperature. The model alloy 0.5 wt.% Fe had ~200.03 MPa yield strength for 60% strain. The alloys were not fully broken, in which the high strain indicated a good ductility of Cu-Ni-based alloy. Furthermore, the addition of a small amount of Fe did not significantly increase the yield strength, as seen in Figure 11(a). However, the addition of 1.5 and 2.5 wt.%Fe caused a slight increase in the alloys' yield strength of 211.67 MPa and 219.01 MPa, respectively. These results were confirmed by the near overlapping line of the compressive yield strength curve. The role of Fe element in increasing strength might originate from their characteristics and the presence of FeNi intermetallic phases formed within the Cu-Ni phases, as observed earlier in XRD spectra (Fig. 9).

The role of warm compaction temperature (150, 200, and 250 °C) of the Cu-Ni-3.0 wt.%Fe alloy on compressive yield strength was investigated in Figure 11(b). Introducing warm compaction in powder metallurgy brought a different response. The highest yield strength of 227.16 MPa has been achieved at the compaction temperature of 150 °C. However, a further increase of the temperature up to 250 °C has been observed to reduce the alloys' yield strength. It is believed that the higher strength was correlated to the constituent elements and intermetallic phase formation in the alloys [40]. The detailed compressive yield

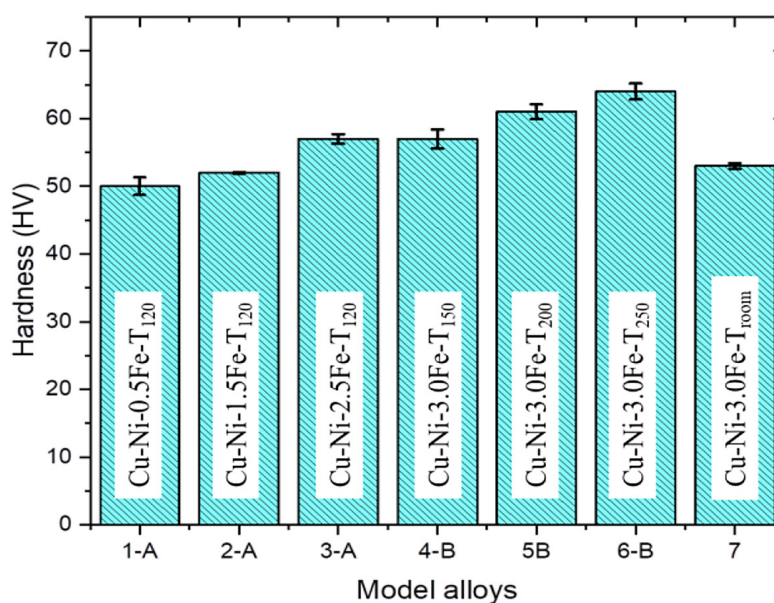


Figure 10. The hardness of the model Cu-Ni-based alloys for different Fe contents and warm compaction temperature

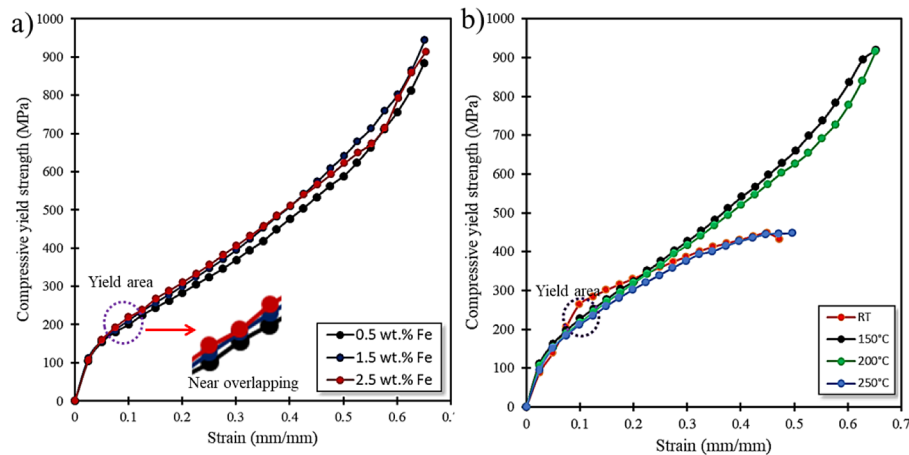


Figure 11. The compressive yield strength of the model Cu-Ni based alloys; (a) a different Fe contents and (b) Cu-Ni-3.0 wt.%Fe with varying warm compaction temperature

strength and standard deviation of the alloy are shown in Table 3.

Higher temperatures have the potential to increase the contaminants dissolved into Cu-Ni-3.0 wt.% Fe green material. Contaminants generated pores and oxides within the microstructure (Fig. 3(d-f)), which decreased the yield strength and strain of the model alloys (Fig. 11(b)). On the other hand, the model alloys with compaction at room temperature show a minimum compressive yield strength. This result corresponded to

the low hardness of the model alloy as shown in Figure 10. Moreover, compressive testing of the model alloy was done at room temperature until fracture occurred. The fracture phenomenon was preceded by grain deformation in the micro-scale of the alloys as shown in Figure 12. Deformation of the Cu-Ni grains was observed perpendicular to the loading direction during the compressive test as seen in Figure 12(b). Figure 12(c) shows the fractured samples where the fracture initiated at the outside diameter of the alloy as

Table 3. The compressive yield strength of the model alloy Cu-Ni-xFe-based alloys

Samples	Model alloys	Compressive yield strength	Deviation	Error
		(MPa)	(MPa)	
1-A	Cu-Ni-0.5Fe-T ¹²⁰	200.0	8.65	0.62
2-A	Cu-Ni-1.5Fe-T ¹²⁰	211.7	5.61	0.38
3-A	Cu-Ni-2.5Fe-T ¹²⁰	219.0	2.84	0.19
4-B	Cu-Ni-3.0Fe-T ¹²⁰	227.1	13.71	0.93
5-B	Cu-Ni-3.0Fe-T ¹⁵⁰	222.2	6.49	0.44
6-B	Cu-Ni-3.0Fe-T ²⁰⁰	184.3	1.52	0.11
7	Cu-Ni-3.0Fe-T ²⁵⁰ room	149.5	22.63	2.00

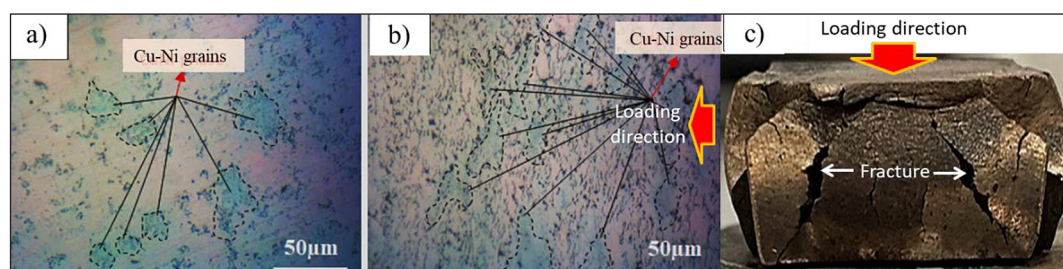


Figure 12. Microstructure of the model Cu-Ni-0.5wt.%Fe alloy; (a) bulk material, (b) after compression test, and (c) fracture of the model alloy

a response to the loading during the compressive yield strength test. Furthermore, fracture morphologies of selected two side fracture surfaces of the Cu-Ni-xFe alloys were observed by SEM. The results are shown in Figure 13(a-d). It is clearly visible that the ductile fractures were predominantly observed in the fracture area of the model Cu-Ni-xFe alloys. This fracture model was confirmed by dimples rupture and fibrous occurred during the compression test.

The ductile fracture also potentially occurred in alloys with solid solution phase, like Cu-Ni-based alloy. In Figure 13(d), intergranular and grain faceted appearance were observed in the Cu-Ni-3.0 wt.%Fe with 250 °C compaction temperature. The fracture models confirmed that the alloy of Cu-Ni-3.0 wt.%Fe with 250 °C compaction temperature had less ductility in comparison with the alloy with lower compaction

temperature. These results corresponded well with the obtained compressive yield strength in Figure 11. Besides the solid solution phase, the fracture morphologies were also influenced by many factors such as oxide formation, second phases, contaminants, and void formation between the microstructures. It is believed that the formation of voids in the microstructure of the alloy influenced the fracture mechanism of the alloys [41]. Void formations were observed in the Cu-Ni-3.0 wt.%Fe as shown in Figure 13(d).

Electrical properties of the model alloys

Table 4 shows the electrical properties of the Cu-Ni-xFe-based alloys with different Fe contents and compaction temperatures. It is clearly observed that the addition of Fe element into Cu-Ni alloys tends to slightly reduce the electrical

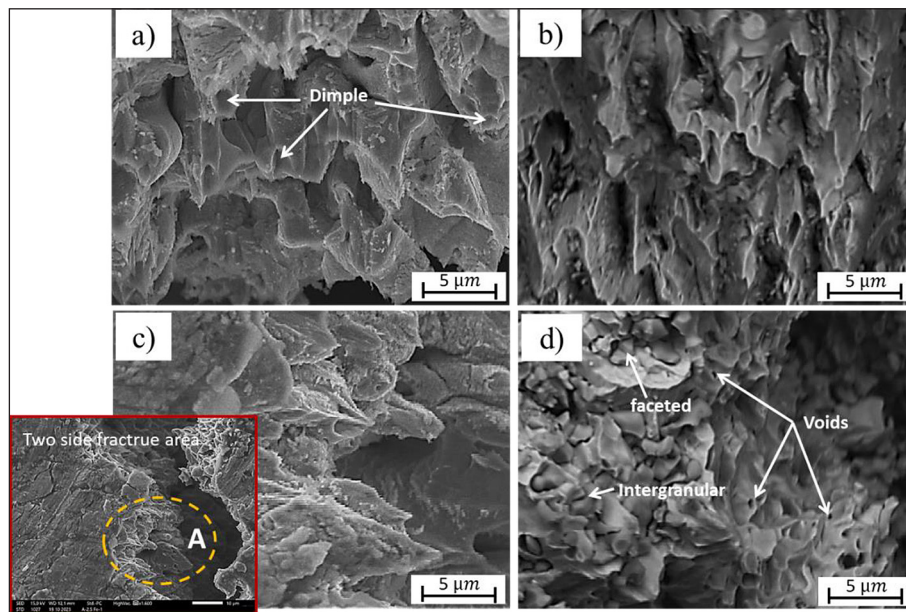


Figure 13. The morphologies of fracture areas of the model alloys; (a) 0.5 wt.%Fe, (b) 1.5 wt.%Fe, (c) 2.5 wt.%Fe at “A” area, and (d) 3.0 wt.%Fe with 250 °C compaction temperature

Table 4. The electrical properties of the model alloy Cu-Ni-xFe-based alloys

Samples	Model alloys	Resistivity	Conductivity	IACS	Deviation
		(Ωm)	(S/m)	(%)	(S/m)
1-A	Cu-Ni-0.5Fe-T ¹²⁰	2.184×10^{-6}	45.79×10^6	76.83	0.30
2-A	Cu-Ni-1.5Fe-T ¹²⁰	2.208×10^{-6}	45.28×10^6	75.97	0.38
3-A	Cu-Ni-2.5Fe-T ¹²⁰	2.215×10^{-6}	45.15×10^6	75.78	0.26
4-B	Cu-Ni-3.0Fe-T ¹²⁰	2.162×10^{-6}	46.25×10^6	77.60	0.35
5-B	Cu-Ni-3.0Fe-T ¹⁵⁰	2.131×10^{-6}	46.92×10^6	78.72	0.72
6-B	Cu-Ni-3.0Fe-T ²⁰⁰	2.122×10^{-6}	47.07×10^6	78.97	0.12
7	Cu-Ni-3.0Fe-T ²⁵⁰ room	2.222×10^{-6}	44.99×10^6	75.63	0.93

conductivity of the alloy. The minimum conductivity of 45.15×10^6 (S/m) was obtained in the alloy with the addition of the 2.5 wt.% Fe. A slight decrease in electrical conductivity with the addition of Fe element into alloys such as Aluminum has been reported [42]. The overall conductivity results show that the presence of Fe reduced the conductivity of Cu-Ni-based alloys. It was potentially caused by their origin of Fe electrical properties that were lower than copper. Furthermore, the introduction of warm compaction in the alloys shows a different effect on their conductivity. The increases in the temperature up to 250 °C improved the electrical properties of the model alloys, in which 78.97% IACS was obtained. This result was higher than 75.63% IACS for Cu-Ni-3.0Fe alloy at room temperature compaction. Therefore, a higher electrical resistivity was obtained at room temperature compaction.

CONCLUSIONS

In this current study, we have investigated the effects of Fe element addition and various compaction temperatures on microstructure, compressive strength, hardness, and electrical properties of the model Cu-Ni-xFe alloys. Based on the results, it can be drawn several conclusions. First, the optical microscope and SEM observation show that the model alloys mainly consisted of Cu-Ni-solid solution phases in their microstructure. However, the addition of the Fe elements in the Cu-Ni-based alloys promotes the inter-metallic phase such as FeNi-phase that strongly influences the alloy hardness. Second, the addition of the Fe element which has a bcc structure also brought a positive effect on the compressive yield strength properties of the Cu-Ni alloys. By the addition of 2.5 wt.% Fe, the increase of yield strength to 219.01 MPa was achieved. However, a slight decrease in the electrical conductivity was obtained by increasing the additional Fe elements. The conductivity decreased from 45.79×10^6 to 45.15×10^6 (S/m) for alloys with additional Fe from 0.5 and 2.5 wt.%, respectively. Lastly, synthesizing model alloys by using a powder metallurgy process with warm compaction conditions successfully improved the alloys' microstructure. The finer particle size of the Cu-Ni-xFe alloys was obtained by introducing the compaction temperature of 150~250 °C, contributing to the increment of alloys' mechanical and electrical

properties. However, a greater compaction temperature probably generates more contaminants, voids, and oxides dissolved into green material, reducing the ductility of model alloys.

Acknowledgments

The authors would like to thank DRTPM, the Ministry of Education, Culture, Research and Technology of the Republic of Indonesia, and Universitas Sumatera Utara which are supporting the funding of this current research through contract No. 36/UN5.4.10.S/PPM/KP-DRTPM/2024.

REFERENCES

1. Hussein SG, Alsaffar I, Al-shammari MA, Al-waily M. Effects of Ni additive on fatigue and mechanical properties of Al-Cu alloy manufactured using powder metallurgy. *J. Eng. Sci. Technol.* 2022;17(5):3310–25. https://jestec.taylors.edu.my/Vol 17 Issue 5 October 2022/17_5_21.pdf
2. Song B, Yu T, Jiang X, Xi W, Lin X. Effect of W content on the microstructure and properties of Cu-Fe alloy. *J. Mater. Res. Technol.* 2020;9(3):6464–74. <https://doi.org/10.1016/j.jmrt.2020.04.031>
3. El-Khatib S., Elsayed AH, Shash AY, El-Habak A. Effect of dispersions of Al_2O_3 on the physical and mechanical properties of pure copper and copper-nickel alloy effect of dispersions of Al_2O_3 on the physical and mechanical properties of pure copper and copper-nickel alloy. *Future Engineering Journal.* 2022;3(1):1–10. <https://digitalcommons.aaru.edu.jo/fej/vol3/iss1/2>
4. Wang M, Yang Q, Jiang Y., Li Z, Xiao Z, Gong S, et al. Effects of Fe content on microstructure and properties of Cu – Fe alloy. *Trans. Nonferrous Met. Soc. China.* 2021;31(10):3039–49. [https://doi.org/10.1016/S1003-6326\(21\)65713-8](https://doi.org/10.1016/S1003-6326(21)65713-8)
5. Marenych O, Kostryzhev A. Strengthening mechanisms in nickel-copper alloys: A review. *Metals.* 2020;10(1358):1–18. <https://doi.org/10.3390/met10101358>
6. Christofidou KA, Robinson KJ, Mignanelli PM, Pickering EJ, Jones NG, Stone HJ. The effect of heat treatment on precipitation in the Cu-Ni-Al alloy Hiduron® 130. *Mater. Sci. Eng. A.* 2017;692(November 2016):192–8. <http://dx.doi.org/10.1016/j.msea.2017.03.069>
7. Weiyang W, Zhu X, Qian LEI, Xiukuang Z, Zhou LI. Research progress of oxide dispersion strengthening copper alloys. *Mater. Sci. Eng. Powder Metall.* 2021;26(6):492–9. <http://doi:10.19976/j.cnki.43-1448/TF.2021067>

8. Li X, Zhang M, Zhang G, Wei S, Wang Q, Lou W, et al. Influence evaluation of tungsten content on microstructure and properties of Cu-W composite. *Metals*. 2022;12(10):1–16. <https://doi.org/10.3390/met12101668>
9. Erçetin A, Aslantaş K. Production of WCu electrical contact material via conventional powder metallurgy method : Characterization, mechanical and electrical properties. *Tr Doğa ve Fen Derg-Tr J Nature Sci*. 2017;6(1). <https://dergipark.org.tr/en/download/article-file/347502>
10. Jiang Y bin, Zhang T tong, Lei Y, HE S Jiang, Liu X hua, Xie J xin. Effects of Ni content on microstructure and properties of aged Cu–0.4Be alloy. *Trans. Nonferrous Met. Soc. China*. 2021;31(3):679–91. [http://dx.doi.org/10.1016/S1003-6326\(21\)65529-2](http://dx.doi.org/10.1016/S1003-6326(21)65529-2)
11. Huang J, Xiao X, Xiong S, Wan J, Guo C. Effect of Ni and Mn contents on the microstructure and properties of Cu–Ni–Mn–P alloy. *J. Alloys Compd*. 2022;901(163636). <https://doi.org/10.1016/j.jallcom.2022.163636>
12. Baroura L, Boukhobza A, Derardja A, Fedaoui K. Study of microstructure and mechanical properties of sintered Fe-Cu alloys. *Int. J. Eng. Res. Afr*. 2018;34(November 2019):5–12. <https://doi.org/10.4028/www.scientific.net/JERA.34.5>
13. Ratov B, Mechnik V, Rucki M, Gevorgyan E, Kilikevicius A, Kolodnitskyi V, et al. Combined effect of CrB₂ micropowder and VN nanopowder on the Strength and wear resistance of Fe–Cu–Ni–Sn matrix diamond composites. *Adv. Sci. Technol. Res. J*. 2023;17(1):23–34. <https://doi.org/10.12913/22998624/157394>
14. Rojas P, Vera R, Martínez C, Villarroel M. Effect of the powder metallurgy manufacture process on the electrochemical behaviour of copper, nickel and copper-nickel alloys in hydrochloric acid. *Int. J. Electrochem. Sci*. 2016;11(6):4701–11. <https://doi.org/10.20964/2016.06.40>
15. Mousapour M, Azadbeh M, Danninger H. Effect of compacting pressure on shape retention during supersolidus liquid phase sintering of Cu base alloys. *Powder Metall*. 2017;60(5):393–403. <https://doi.org/10.1080/00325899.2017.1357781>
16. Zhang Y, Guo X, Chen Y, Li Q. Effect of compaction pressure on the densification, microstructure, and mechanical properties of Ti-1Al-8V-5Fe alloy based on TiH₂ and HDH-Ti powders. *Micro Nano Lett*. 2019;14(8):906–10. <https://doi.org/10.1049/mnl.2018.5736>
17. Meyer YA, Bonatti RS, Costa D, Bortolozzo AD, Osório WR. Compaction pressure and Si content effects on compressive strengths of Al/Si/Cu alloy composites. *Mater. Sci. Eng. A*. 2020;770:1–7. <https://doi.org/10.1016/j.msea.2019.138547>
18. Sabri AM, Rahim MZ, Ahmad MAH, Azis NH, Ibrahim MR, Mubarak A, et al. The effect of powder metallurgy parameters on electrical conductivity of copper-nickel-tungsten electrode. *Int. J. Eng. Technol*. 2019;8:111–6. <https://doi.org/10.14419/ijet.v8i1.1.24788>
19. Huang JS, Min S. Preparation of Fe-Cu-Ni-Mo-C alloy with high performance by powder metallurgy warm compaction. *Adv. Mater. Res*. 2011;194–196:100–3. <https://doi.org/10.4028/www.scientific.net/AMR.194-196.100>
20. Feng SS, Geng HR, Guo ZQ. Effect of lubricants on warm compaction process of Cu-based composite. *Compos. B: Eng*. 2012;43(3):933–9. <https://doi.org/10.1016/j.compositesb.2011.09.004>
21. Ibrahim MHI, Abdul Razak MI, Mustafa N, Selamat MA. Carbon-Copper (C-CU) composites using local carbon material through warm compaction process for potential electrical and electronic applications. *ARPN J. Eng. Appl. Sci*. 2016;11(18):11117–23. http://www.arpnjournals.org/jeas/research_papers/rp_2016/jeas_0916_5044.pdf
22. Wang P, Zhu Z, Liu J, Wang H, Pang J, Zhang J. Finemet nanocrystalline magnetic powder cores: Application of binder and warm compaction process. *J. Magn. Magn. Mater*. 2024;596:171985. <https://doi.org/10.1016/j.jmmm.2024.171985>
23. Huang H, Zhang R, Sun H, Zhang J, Wang J. High density Fe-based soft magnetic composites with nice magnetic properties prepared by warm compaction. *J. Alloys Compd*. 2023;947(169460):1–10. <https://doi.org/10.1016/j.jallcom.2023.169460>
24. Nassef A, El-Garaihy WH, El-Hadek M. Characteristics of cold and hot pressed iron aluminum powder metallurgical alloys. *Metals*. 2017;7(5). <https://doi.org/10.3390/met7050170>
25. Omar HD. The analysis of copper-iron metallic mixture by means of XRD and XRF. *International Letters of Chemistry, Physics and Astronomy*. 2016;64:130–4. <https://doi.org/10.56431/p-tj32k9>
26. Karnati S, Liou FF, Newkirk JW. Characterization of copper – nickel alloys fabricated using laser metal deposition and blended powder feedstocks. *Int. J. Adv. Manuf. Tech*. 2019;103:239–50. <https://doi.org/10.1007/s00170-019-03553-0>
27. Shang X, Wang X, Chen S. Effects of ball milling processing conditions and alloy components on the synthesis of Cu-Nb and Cu-Mo alloys. *Materials*. 2019;12(8):1–9. <https://doi.org/10.3390/ma12081224>
28. Dong D, Duan L, Cui J, Li G, Jiang H, Pan H. Influence of compaction temperature on the mechanical properties and micro morphology of Cu / CNTs composites prepared by electromagnetic impacting. *Powder Technol*. 2022;396:433–43. <https://doi.org/10.1016/j.powtec.2021.11.014>
29. Majzoobi GH, Bakhtiari H, Atrian A, Pipelzadeh MK, Hardy S. Warm dynamic compaction of Al6061/SiC nanocomposite powders. *Proc. Inst.*

- Mech. Eng. Pt. L J. Mater. Des. Appl. 2015;230:1–13. <https://doi.org/10.1177/1464420714566628>
30. Singh R, Sharma AK, Sharma AK. Physical and mechanical behavior of NiTi composite fabricated by newly developed uni-axial compaction die. Mater. Res. 2021;24(3). 1–10. <https://doi.org/10.1590/1980-5373-MR-2020-0549>
31. Zhou Y, Wang J. Mechanical properties of thermally annealed Cu/Ni and Cu/Al multilayer thin films: Solid solution vs. intermetallic strengthening. Metals. 2024;14:1–12. <https://doi.org/10.3390/met14030256>
32. Çelik E, Aslan AK. The effect of porosity and cure on microstructure and mechanical properties of co alternative powder metallurgy compound. Sci. Sinter. 2017;49(3):225–34. <https://doi.org/10.2298/SOS1703225C>
33. Xing H, Hu P, Han J, Li S, Ge S, Hua X. Effects of oxygen on microstructure and evolution mechanism of body-centred-cubic molybdenum. Int. J. Refract. Met. Hard Mater. 2022;103:105747. <https://doi.org/10.1016/j.ijrmhm.2021.105747>
34. Moser M, Lorand S, Bussiere F, Demoisson F, Couque H, Bernard F. Influence of carbon diffusion and the presence of oxygen on the microstructure of molybdenum. Metals. 2020;10(948):1–17. <https://doi.org/10.3390/met10070948>
35. Spilker B, Linke J, Pintsuk G, Wirtz M. Oxide segregation and melting behavior of transient heat load exposed beryllium. Nucl. Fusion. 2016;56:1–9. <https://doi.org/10.1088/0029-5515/56/10/106014>
36. Jiao X, Zhang Y, Wu Q, Shang Z, Yu Y. High-temperature oxidation behavior and pore structure of porous TiAl₃ intermetallics at 650 °C to 900 °C. J. Mater. Res. Technol. 2023;22:2398–408. <https://doi.org/10.1016/j.jmrt.2022.12.074>
37. Li Q, Liu Z, Liu X, Wang L, Zang C, Li L, Rivera-Diaz P.E.J, del-Castillo. Enabling Invar to Ti6Al4V transitions through copper in functionally graded laser powder bed fused components. J. Mater. Res. Technol. 2024;32:2595–608. <https://doi.org/10.1016/j.jmrt.2024.08.122>
38. Chang C.C., Wu M.R. Effects of particle shape and temperature on compaction of copper powder at micro scale. In: International Conference on Precision Machinery and Manufacturing Technology. Kending, Taiwan: MATEC Web of Conferences; 2017. <https://doi.org/10.1051/mateconf/201712300011>
39. Wang D, Li M, An X. Numerical study on the warm compaction and solid-state sintering of TiC / 316L composite powders from particulate scale. Powder Technol. 2022;402:1–19. <https://doi.org/10.1016/j.powtec.2022.117361>
40. Necas D, Marek I, Pinc J, Vojtech D, Kubásek J. Advanced zinc – magnesium alloys prepared by mechanical alloying and spark plasma sintering. Materials. 2022;15:1–17. <https://doi.org/10.3390/ma15155272>
41. Wciślik W, Lipiec S. Void-induced ductile fracture of metals: Experimental observations. Materials. 2022;15(18). <https://doi.org/10.3390/ma15186473>
42. Jabłoński M, Knych T, Mamala A, Smyrak B, Wojtaszek K. Influence of Fe And Si addition on the properties and structure conductivity aluminium. Arch Metall Mater. 2017;62(3):1541–1547. <https://doi.org/doi.10.1515/amm-2017-0237>